Reconfigurable phased antenna array for extending cubesat operations to Ka-band: Design and feasibility

G. Buttazzoni[a], M. Comisso[a,*], A. Cuttin[a], M. Fragiacomo[b], R. Vescovo[a], R. Vincenti Gatti[c]

[a] Dept. of Engineering and Architecture, Univ. of Trieste, Via A. Valerio 10, Trieste, Italy
[b] PicoSaTs s.r.l., Area Science Park, Padriciano 99, 34149 Trieste, Italy
[c] Dept. of Engineering, Univ. of Perugia, Via G. Duranti 93, 06125 Perugia, Italy

ARTICLE INFO

Keywords:
CubeSat
Ka-band
Phased-array
Reconfigurability

ABSTRACT

Started as educational tools, CubeSats have immediately encountered the favor of the scientific community, subsequently becoming viable platforms for research and commercial applications. To ensure competitive data rates, some pioneers have started to explore the usage of the Ka-band beside the conventional amateur radio frequencies. In this context, this study proposes a phased antenna array design for Ka-band downlink operations consisting of 8×8 circularly polarized subarrays of microstrip patches filling one face of a single CubeSat unit. The conceived structure is developed to support 1.5 GHz bandwidth and dual-task missions, whose feasibility is verified by proper link budgets. The dual-task operations are enabled by a low-complexity phase-only control algorithm that provides pattern reconfigurability in order to satisfy both orbiting and intersatellite missions, while remaining adherent to the cost-effective CubeSat paradigm.

1. Introduction

In the last decade, a growing number of small satellites has populated the Low-Earth Orbit (LEO), specifically involving a recently developed class of spacecrafts, called CubeSats [1]. The structure of an N-Unit (NU) CubeSat is made up of N cubic units, each having a volume of 1 dm^3, which contain one or more systems of the satellite. Common form factors are 1U, 2U, and 3U [1], even though a recent upgrade has enlarged the possible overall dimensions to 6U, 12U, and even 27U [2]. The CubeSat concept was initially thought as a mean to provide hands-on experience in the field of spacecraft technology for educational and scientific purposes [3]. At this first stage, the amateur radio bands were considered sufficient for the support of the communications. In a short time, however, CubeSats started to attract conspicuous investments from military, government, and commercial organizations, thanks to the increased availability of off-the-shelf components and launches at reduced cost. This has determined the need of larger transfer rates, inviting the exploration of the Ka-band beside the conventional S and X ones [4–6]. Unfortunately, the Ka-frequencies are characterized by strong attenuations, whose compensation requires the use of high-performance antennas specifically designed to satisfy the stringent constraints of the CubeSat technology.

In this context, some proposals have been formulated. The Jet Propulsion Laboratory has recently developed an attractive high-gain Ka-band parabolic antenna, realized adopting 30 ribs stowed within a space of 1.5U that unfold to deploy the antenna in a Cassegrain configuration [7]. In [8], a conical horn has been embedded onto the 1U envelope of the transmitter. A cutting-edge reflectarray antenna operating at 26 GHz and printed on the back of three deployable solar panels has been designed within the Integrated Solar Array and Reflectarray Antenna (ISARA) mission, sponsored by the NASA Small Satellite Technology Program [9].

Beside these projects under development, further interesting solutions may derive from antenna array technology, which has however received less consideration, even if, nowadays, reflectors and arrays compete in many types of systems [10]. Several motivations invite to essay this possibility: compactness, no aperture blockages, and avoidance of deployment phases, since an array of microstrip patches may be directly embedded on a CubeSat face. Flexibility can also be guaranteed by implementing a suitable beamforming algorithm able account for multiple requirements, including high-gain and Circular Polarization (CP): two features that are in practice mandatory to limit the strong signal attenuation and the polarization mismatch. Other functionalities, such as phase-only control and pattern reconfigurability, may be introduced to simplify the actual realization of the feeding network and to support possible multi-task missions. Forthcoming missions, in fact,

* Corresponding author.
E-mail addresses: gbuttazzoni@units.it (G. Buttazzoni), mcomisso@units.it (M. Comisso), alessandro.cuttin@phd.units.it (A. Cuttin), vescovo@units.it (M. Fragiacomo), mariofragiacomo@picosats.eu (R. Vescovo), roberto.vincentigatti@unipg.it (R. Vincenti Gatti).

Accepted 9 April 2017

will not be limited to conventional LEO orbiting, requiring high-gain narrow-beam antenna patterns, but are also expected to involve constellations of CubeSats [11,12], requiring patterns with wider main lobes to enable the identification of other nearby CubeSats for intersatellite communication purposes.

In light of these considerations, this paper presents the design of a Ka-band phased antenna array providing CP and pattern reconfigurability to support downlink and intersatellite CubeSat missions. Preliminary experimental and numerical results combined with illustrative link budgets are also reported to discuss the applicability of the array technology to next generation Ka-band CubeSats.

The paper is organized as follows. Section 2 presents the array structure. Section 3 introduces the reconfiguration functionalities. Section 4 discusses the feasibility aspects. Section 5 remarks the most relevant conclusions.

2. Array structure

Since the design of spacecraft subsystems is strictly dependent on the mission objectives, we consider, as a baseline for the development of the array structure, a broadside configuration, which can be suitably adapted to different tasks. With this choice, in this section, we first design the array structure by accounting for the operational frequency and the size constraints, while, in Section 3, we synthesize the required radiation patterns by accounting for the mission purposes.

The array structure consists of a planar array that fits to one face of a 1U CubeSat [14], so as to make the proposed antenna system suitable for missions adopting any of the allowed form factors from 1U to 27U. A mechanical prototype built at PicoSaTs s.r.l. [13], displays the face chosen to accommodate the array (Fig. 1), which consists of N subarrays, each formed by four microstrip patches. The design of the subarray with the corresponding parameters is reported in Fig. 2(a) and (b). The single patch, realized to operate in the Ka-band at the frequency of 37 GHz, corresponding to a wavelength $\lambda = 8.108$ mm, is developed using the mitering method [15], to obtain Right-Hand CP (RHCP) [16]. For manufacturing reasons and to reduce the coupling effects with the feeding line due to the high operational frequency, a three-layer design is considered, with two DiClad 880 substrates and a mid prepreg I-TERA MT solding substrate. To better match the RHCP constraint, minimize Left-Hand CP (LHCP), and to increase the bandwidth, the subarray building block is developed using the sequential phase-rotation technique by sequentially arranging the four patches in orientation and phase at 0°, 90°, 180°, and 270° [17,18]. The sequential phases are achieved by quarter-wavelength delay lines and optimizing the feeding network by CST Microwave Studio to minimize the losses. In particular, the lengths $a_1,\ldots,a_4$ in Fig. 2(a) are evaluated to ensure that the relationships $a_2 + a_4 - \lambda_g/4 = a_1 + a_4 = a_2 + a_3 + \lambda_g/4 = a_1 + a_3 + \lambda_g/2$ be satisfied for the guided wavelength $\lambda_g = 5.616$ mm.

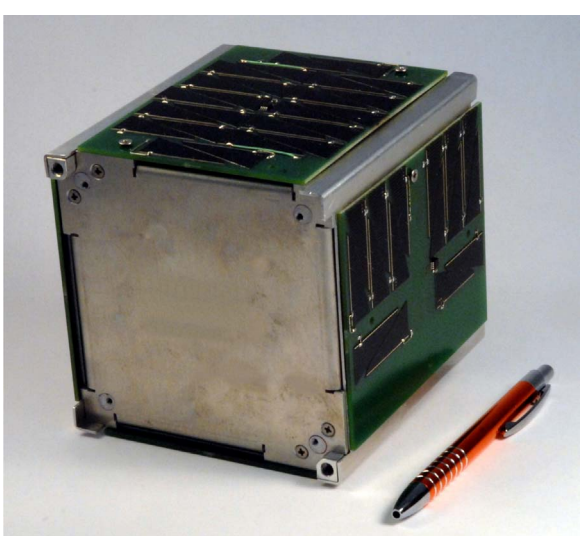

Fig. 1. Mechanical mock-up of a 1U CubeSat: the exposed face of the frame (i.e., the one without solar panels) is selected to accommodate the developed antenna array. Picture courtesy of PicoSaTs s.r.l. [13].

The simulated and experimental performance obtained from a fabricated prototype (Fig. 3), shows that the subarray provides a 10 dB-bandwidth larger than 1.5 GHz (Fig. 4(a)), thus matching the high-bandwidth requirement, and a maximum gain of 11.54 dB with an RHCP/LHCP isolation of 12.51 dB (Fig. 4(b) and (c)). A satisfactory level of polarization purity is also obtained, since both the simulated and measured Axial Ratios (ARs) remain within 3 dB in the mainlobe. Except for few discrepancies in the $\varphi = -90°$ half-plane (Fig. 4(c)) due to a partially unshielded cable connector on the back of the prototype, a good agreement between simulations and measurements may be observed.

For the design of the full array, the surface that can be actually occupied at the net of the mandatory CubeSat rails [1], is a square of edge R=85 mm. Since the maximum size of a subarray is u_x=9.024 mm (Fig. 2(a)), an array of $N = 8 \times 8 = 64$ elements may be placed on the available surface by selecting a distance r=10.625 mm between the feeding points of two adjacent subarrays, in order to maintain a distance of at least $\lambda/5$ between their sides (Fig. 5). To account for the mutual coupling due to the closeness between the elements, the ϑ-(zenith) and φ-(azimuth) components $E_n^{\vartheta}(\Omega)$ and $E_n^{\varphi}(\Omega)$ of the electric far-field of the n-th subarray (n=1,...,N) in the direction $\Omega = (\vartheta, \varphi)$ are calculated accounting for the presence of the other adjacent subarrays by using the method in [19]. This method exploits the linear relationship between the array and the element patterns to estimate $E_n^{\vartheta}(\Omega)$ and $E_n^{\varphi}(\Omega)$ by a suitable electromagnetic software (in our case CST Microwave Studio) using a unity-voltage zero-phase feed for the n-th element and a zero-voltage feed for the remaining $N-1$ elements. Besides, to obtain a compact formulation, $E_n^{\vartheta}(\Omega)$ and $E_n^{\varphi}(\Omega)$ include also the phase shift due to the position inside the array. Hence, denoting as j the imaginary unit and as $\boldsymbol{\alpha} = [\alpha_1,\ldots,\alpha_N]$ the vector of the complex excitations of the array elements, the RHCP component $E_1(\boldsymbol{\alpha}; \Omega)$ and the LHCP component $E_2(\boldsymbol{\alpha}; \Omega)$ are jointly expressed, for i=1,2, as:

$$E_i(\boldsymbol{\alpha}; \Omega) = \frac{1}{\sqrt{2}} \sum_{n=1}^{N} \alpha_n [E_n^{\vartheta}(\Omega) - j(-1)^i E_n^{\varphi}(\Omega)], \tag{1}$$

which analytically describes the RHCP/LHCP patterns provided by the array structure for a given excitation vector $\boldsymbol{\alpha}$.

3. Pattern synthesis

Once the array structure is designed, the excitations of the N subarrays are synthesized to generate two different patterns for supporting a dual-task mission. Next-generation CubeSats are in fact expected to perform not only LEO orbiting, but also internetworking operations, where constellations of small satellites exchange scientific or commercial data. Accordingly, a task t=1 consists in communicating with the ground station by a pattern with a narrow, high-gain beam. A task t=2 consists in realizing an intersatellite link, which takes advantage of a pattern with a broader beam and a lower gain to properly search the neighboring CubeSats. The aim is to satisfy the generic task t by simply orienting the CubeSat face containing the array towards the appropriate region of space (i.e., towards the ground station for t=1, or towards the satellites' constellation for t=2) by means of the on-board Attitude Determination and Control Subsystems (ADCSs), and then selecting the proper excitation vector $\boldsymbol{\alpha}_t = [\alpha_{1,t},\ldots,\alpha_{N,t}]$. Thus, two sets of excitations, $\boldsymbol{\alpha}_1$ and $\boldsymbol{\alpha}_2$, must be synthesized to enable the reconfigurability of the pattern according to

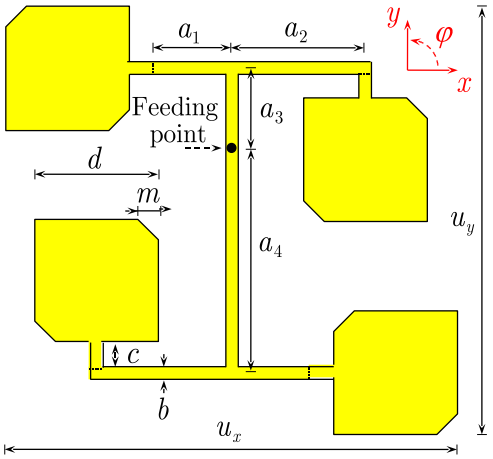

Parameter	Value [mm]
d	2.512
m	0.675
c	0.500
b	0.250
a_1	1.500
a_2	2.904
a_3	1.516
a_4	4.324
u_x	9.024
u_y	8.352

(a)

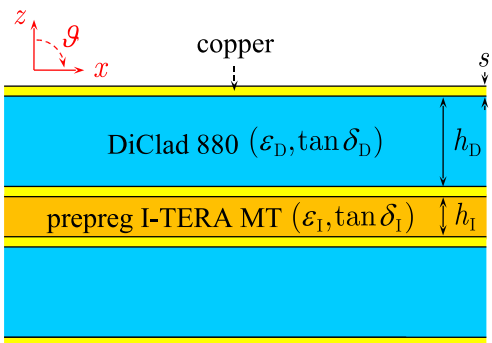

Parameter	Value
s	0.035 mm
h_D	0.254 mm
ε_D	2.20
$\tan\delta_D$	0.0009
h_I	0.065 mm
ε_I	3.45
$\tan\delta_I$	0.0031

(b)

Fig. 2. Subarray building block: (a) front-view design, (b) side-view design.

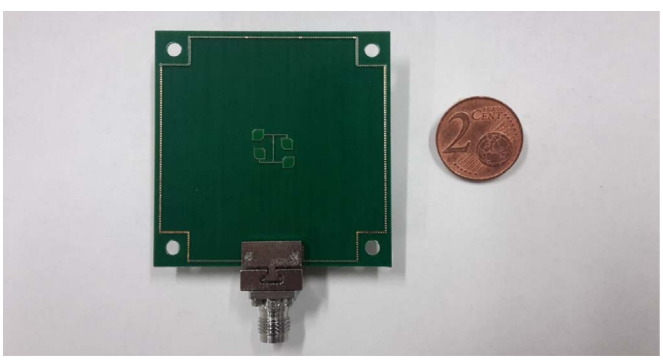

Fig. 3. Subarray building block: fabricated prototype.

the selected task. For each task, the LHCP field represents the undesired radiation, so its amplitude is kept below a given threshold ζ_t. Furthermore, the amplitude $|\alpha_{n,t}|$ and the phase $\arg(\alpha_{n,t})$ of the n-th element during the task t are properly constrained to reduce the complexity of the feeding network. More precisely, $|\alpha_{n,t}|$ is forced to belong to the set $\{0, 1\}$ (on/off condition), thus, all the actually active elements have an identical amplitude, and the synthesis is hence carried out by phase-only control. In summary, the formulated dual-task problem consists in finding, for each t=1,2 value, an excitation vector $\boldsymbol{\alpha}_t$ satisfying the constraints:

$$|E_1(\boldsymbol{\alpha}_t; \Omega)| \in M^t, \tag{2a}$$

$$|E_2(\boldsymbol{\alpha}_t; \Omega)| \leq \zeta_t, \tag{2b}$$

$$|\alpha_{n,t}| \in \{0, 1\}, \; n = 1, \ldots, N, \tag{2c}$$

where M^t is the RHCP pattern mask that imposes the desired maximum gain $\mathcal{G}_t$, side-lobe level (SLL) ρ_t, and Half-Power BeamWidth (HPBW) ω_t for the task t. In particular, the imposed values are $\mathcal{G}_1 = 25$ dB, $\rho_1 = \zeta_1 = 15$ dB, $\omega_1 = 4°$, (task 1, narrow beam and high gain), $\mathcal{G}_2 = 15$ dB, $\rho_2 = \zeta_2 = 5$ dB, $\omega_2 = 20°$ (task 2, wider beam and lower gain). This problem is solved by first identifying two sets: a set U, whose elements satisfy conditions (2a)–(2c), and a set V, whose elements account for the array structure by (1). Then, the algorithm in [20] is applied to perform an iterative sequence of alternate projections onto U and V to find the $\boldsymbol{\alpha}_1$ and $\boldsymbol{\alpha}_2$ vectors that minimize the distance between the two sets. The synthesized excitation phases are realized by the feeding network in Fig. 6. The integer k near each subarray feeding point identifies the derived phase shift $\chi_k = k\pi/8$ (quantized to a multiple of $\pi/8$ to simplify the actual realization), which has been implemented by a stripline of length $\Delta_k = \chi_k/(2\beta_g) = k\lambda_g/32$, being $\beta_g = 2\pi/\lambda_g$ the wave number referred to the guided wavelength. Two switches are also inserted to enable pattern reconfigurability, since all elements are active for t=1, while just the four ones inside the dashed square are active for t=2. To maintain the phasing of the feeding network for t=1, the second switch is provided with a properly designed delay line of length Δ_f.

Fig. 7 reports the simulated performance of the full structure (array and feeding network). In particular, Fig. 7(a) shows that the reconfigurable array maintains a satisfactory return loss, providing, for t=1 (Fig. 7(b)), a maximum gain of 24.04 dB, an HPBW of 4°, an LHCP/RHCP isolation of 13.47 dB, an AR of 3.75 dB, and, for t=2 (Fig. 7(c)), a maximum gain of 13.28 dB, an HPBW of 20°, an LHCP/RHCP isolation of 13.33 dB, an AR of 3.80 dB. Thus, it guarantees, beside the gain, a satisfactory polarization purity also for the second task, characterized by a wider mainlobe. These results confirm that a

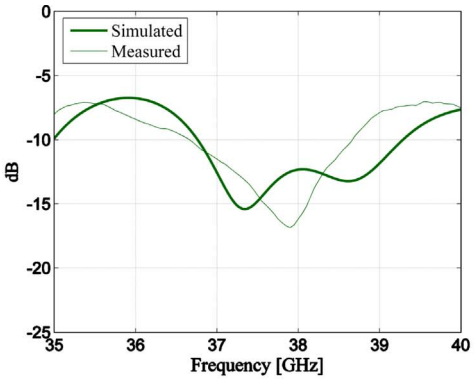

(a)

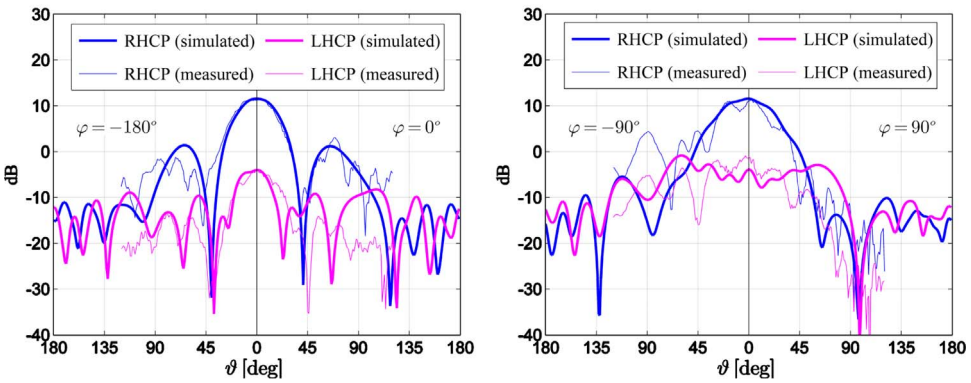

(b) (c)

Fig. 4. Subarray performance: (a) return loss, (b) 2D gain pattern cuts in the $x - z$ plane, (c) 2D gain pattern cuts in the $y - z$ plane.

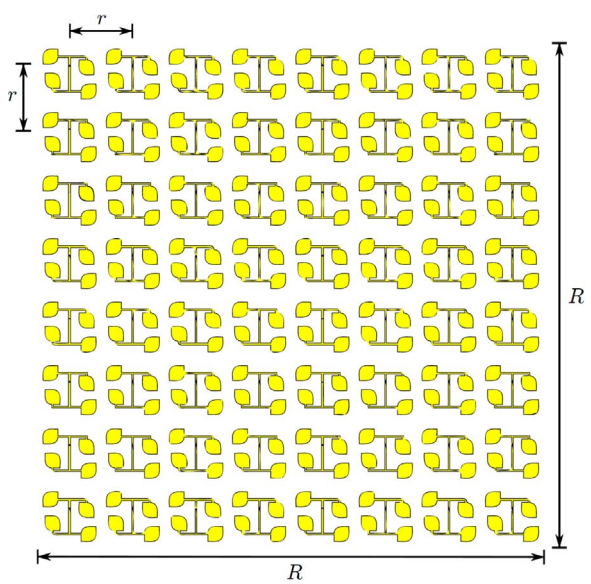

Fig. 5. Array structure: front view.

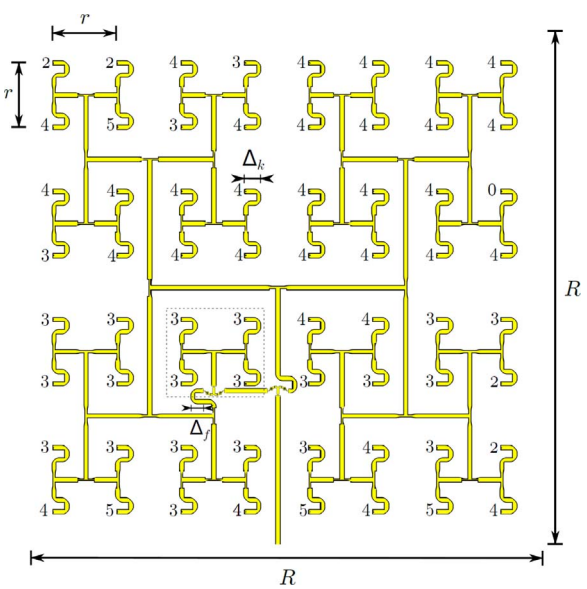

Fig. 6. Array structure: back view (feeding network).

reconfigurable antenna array embedded on a CubeSat face may be able to satisfy the pattern requirements of forthcoming dual-task missions.

4. Feasibility aspects

To get a clearer view of the actual applicability of the designed reconfigurable Ka-band array in CubeSat scenarios, some specific implementation aspects relative to the link budgets and the competing reflectarray technology deserve to be investigated in more detail.

4.1. Link budgets

The discussion moves from two illustrative link budgets, which are developed for the two considered tasks: the CubeSat-ground station downlink (Table 1) and the intersatellite communication (Table 2). Even though the two tasks have some common parameters and the corresponding budgets may look similar at a first glance, they exhibit significant differences when it comes to the evaluation of the propagation losses and receivers' features.

Once the input power and the transmitting antenna parameter (that

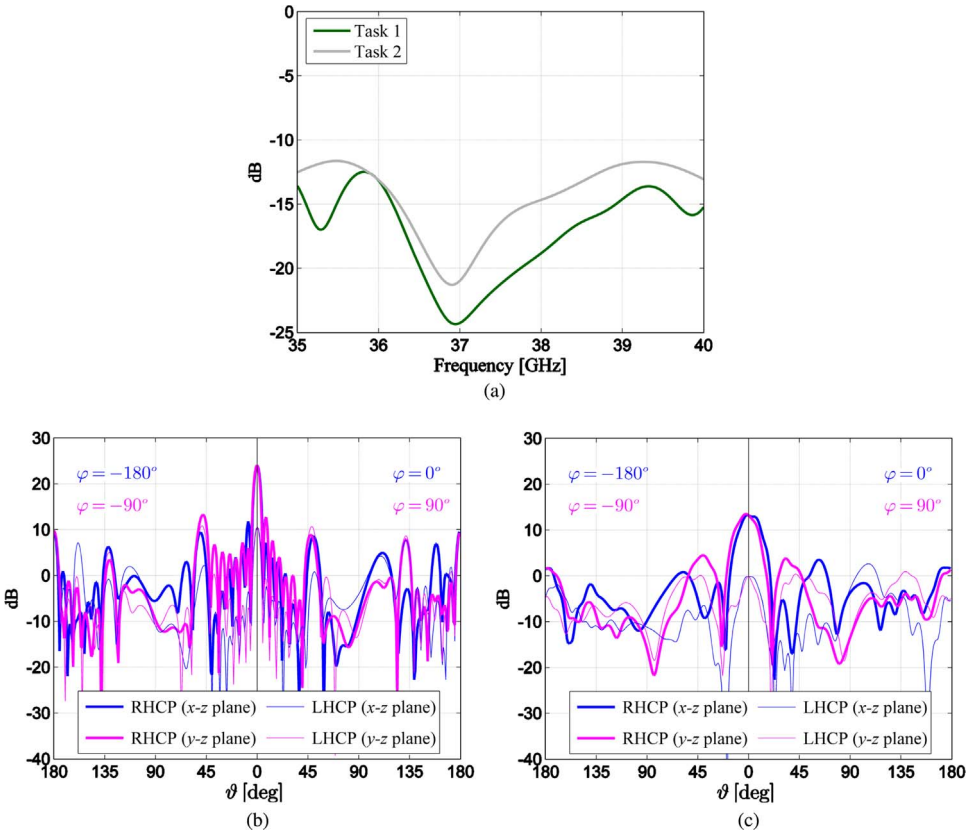

Fig. 7. Reconfigurable array performance: (a) return loss, (b) 2D gain pattern cuts for task 1, (c) 2D gain pattern cuts for task 2.

is, the gain in the presence of the feeding network, the HPBW, and the polarization losses), are established for each task, a detailed link budget at the spacecraft side has to account for the pointing accuracy. Since the antenna is conceived to fit on a face of the spacecraft, its pointing is expected to be provided by the ADCS. Commercially available ADCSs typically provide a pointing accuracy of 0.5° or better [22], thus the impact of the pointing losses on the Effective Isotropic Radiated Power (EIRP) is limited for both tasks.

The propagation path is the major responsible for the losses, which shall be compensated by the transmitting and receiving subsystems. Whereas, in the intersatellite link, it is safe to assume that the overall path losses are given mainly by the Free Space Path Loss (FSPL), this is not the case for the downlink from space to Earth, where additional attenuations come into play because of the presence of the Earth's atmosphere. Moreover, given the low-earth orbit, the performance of the link during the access is not uniform, because the slant range between the ground station and the spacecraft varies from 400 km at the zenith to over 2000 km at the horizon, therefore yielding a significant variation of the FSPL during the in-view period. To take this into account, the budget for task 1 presents as a reference the average value of the FSPL corresponding to the average distance, meaning that the margin will improve when the satellite approaches the zenith, and will worsen when the satellite is closest to the horizon. Also, it may be noticed that the additional atmospheric attenuations in Table 1 relative to rain and clouds hold in pessimistic faded scenarios, while, in clear sky conditions, these attenuations are considerably reduced, thus increasing the available margin.

At the receiving end, in the task 1, the antenna is considered to be a parabolic reflector with a 70% efficiency and a pointing accuracy of 0.1° [25], while, in the task 2, it is considered as an antenna system identical to the transmitting one. Distinct environmental conditions, referred to the Earth surface (task 1) and to the exosphere (task 2), are experienced by the two receiver sides, thus considerably differentiating the corresponding system noise temperatures even in the presence of an identical receiver. For both tasks, the selected receiver exploits one of the novel MODulation-CODe (MODCOD) configurations offered by the recently released Digital Video Broadcasting (DVB)-S2X extension [27]. This amendment extends the Signal-to-Noise Ratio (SNR) working conditions with respect to the original DVB-S2 standard, until −10 dB, thus allowing the connectivity in the presence of significant atmospheric absorptions, which may sometimes arise during Ka-band communications. In particular, the receiver sides of the developed link budgets rely on the newly available configuration consisting of a quadrature phase-shift keying modulation in combination with a low density parity check/Bose Chaudhuri Hocquenghem joint encoder of rate 2/9, which ensures a reliable communication at 100 Mbps [26]. This choice, considered in conjunction with the available SNR resulting from the designed antenna system, leaves a satisfactory link margin for both tasks. To this purpose, it should also be noted that the selected communication protocol supports the adaptive coding and modulation, thus potentially allowing the full exploitation of the excess link margin by activating higher throughput MODCODs that require higher $(E_b/N_0)^r$ values. From a technological point of view, the premises to adopt a Ka-band communication link with the DVB-S2X standard are already in place. One proposal for a Ka-band CubeSat transceiver is presented in [28], and consists in mixing an intermediate-frequency signal at 1 GHz with the second harmonic generated by a local oscillator operating at half of the desired radio-frequency. Exploiting this approach, the presence on the market of components operating at frequencies beyond 15 GHz enables the achievement of frequencies above 30 GHz [29]. A second proposal, offering a range of operating frequencies between 17 and 40 GHz, relies on a software defined radio platform [30], thus allowing the upgrade to the advanced MODCODs specified in the DVB-S2X standard. In this context, an antenna array seems hence perfectly suited for enabling the support of dual-task missions in next generation Ka-band nanosatellites.

4.2. Arrays and reflectarrays

The applicability of phased-arrays to Ka-band CubeSats may be further deepened by considering the competing antenna technology based on reflectarrays [10]. In this field, the most advanced solution is the ISARA proposal, for which, even if the project is still under development, some preliminary numerical results are already available [9]. A comparative description of these two systems may be useful to better outline benefits and drawbacks of each technology in terms of mechanics, losses, versatility, and space available for the solar cells.

From a mechanical point of view, both antenna systems do not occupy space inside the CubeSat before the launch (except for the small packaged feed of ISARA), thus leaving more volume available to the other subsystems. ISARA requires the mechanical deployment of the panels and of the feed, which might represent a critical phase of the mission that may suffer from vibrations, heat variations, or other possible mechanical setbacks due to the launch or the space environment. Conversely, the array solution is ready to be operated as it is integrated on the spacecraft, without requiring any further intervention to be serviceable.

From the point of view of the losses, arrays are not subject to spillover (anyway minimized in the ISARA design), feed package loss, and aperture blockage, which, according to the currently available design, may instead partly affect ISARA because the feed and part of the CubeSat envelope may be not completely outside of the reflectarray aperture ([9], Fig. 1). However, these three factors, even combined, have in general an impact lower than that of the losses, due to the feeding network and the patch substrates, that characterize antenna arrays. This difference provides large benefits to ISARA, which achieves a gain of 33 dB with a 3U CubeSat. A fair comparison should anyway consider that the presented phased-array relies on a 1U CubeSat to provide a basic module, which might be replicated on more faces of an NU spacecraft to increase the gain.

From the versatility point of view, phased-arrays may be employed to support multi-task missions by pattern reconfigurability. A possibility exploited in the presented design, but not even considered in the ISARA proposal.

Finally, from the point of view of the space available for the solar cells, one may observe that the solar panels printed on the back of the ISARA reflectarray cover an area equivalent to nine 1U CubeSat faces, while five 1U CubeSat faces are available for solar panels in the proposed design. However, a scaling of the developed phase-array to a 3U CubeSat, reveals that, even considering three faces covered by three replicas of the array, eleven faces would remain accessible to solar cells. Therefore, the compactness and the conformability of the phased-array do not imply limitations for the energy supply of the CubeSat system.

Table 1
Link budget for task 1 (CubeSat-ground station downlink).

Spacecraft and transmitting (designed) antenna	
Input power: P	0.00 dBW
Line losses: L^{l}	0.10 dB
Maximum antenna gain: $G_{\mathrm{t},1}$	24.04 dB
Antenna HPBW: $\Omega_{\mathrm{t},1}$	4.00°
Antenna polarization losses: $L^{\mathrm{x}}_{\mathrm{t},1}$ [21]	0.19 dB
Pointing accuracy: e_{t} [22]	0.50°
Pointing losses: $L^{\mathrm{p}}_{\mathrm{t},1} = 12(e_{\mathrm{t}}/\Omega_{\mathrm{t},1})^2$ [23]	0.19 dB
Antenna effective gain: $G^{\mathrm{e}}_{\mathrm{t},1} = G_{\mathrm{t},1} - L^{\mathrm{x}}_{\mathrm{t},1} - L^{\mathrm{p}}_{\mathrm{t},1}$	23.66 dB
$\mathrm{EIRP}_1 = P - L^{\mathrm{l}} + G^{\mathrm{e}}_{\mathrm{t},1}$	23.56 dBW
Downlink path	
Average distance: D_1	1200.00 km
$\mathrm{FSPL}_1 = 20\log_{10}(4\pi D_1/\lambda)$ [24]	185.40 dB
Atmospheric gases attenuation: L^{g} [24]	5.00 dB
Rain attenuation: L^{w} [24]	2.00 dB
Cloud attenuation: L^{c} [24]	2.00 dB
Scintillation: L^{k} [24]	2.00 dB
Total path attenuation: $L^{\mathrm{a}}_1 = \mathrm{FSPL}_1 + L^{\mathrm{g}} + \sqrt{L^{\mathrm{w}} + L^{\mathrm{c}} + L^{\mathrm{k}^2}}$ [24]	193.22 dB
Ground station and receiving reflector antenna	
Antenna diameter: ξ	1.00 m
Antenna efficiency: η	0.70
Maximum antenna gain: $G_{\mathrm{r},1} = 10\log_{10}[\eta(\pi\xi/\lambda)^2]$ [23]	50.22 dB
Antenna HPBW: $\Omega_{\mathrm{r},1} = 70\lambda/\xi$ [23]	0.57°
Antenna polarization losses: $L^{\mathrm{x}}_{\mathrm{r},1}$ [21]	0.35 dB
Antenna pointing accuracy: $e_{\mathrm{r},1}$ [25]	0.10°
Pointing losses: $L^{\mathrm{p}}_{\mathrm{r},1} = 12(e_{\mathrm{r},1}/\Omega_{\mathrm{r},1})^2$ [23]	0.37 dB
Antenna effective gain: $G^{\mathrm{e}}_{\mathrm{r},1} = G_{\mathrm{r},1} - L^{\mathrm{x}}_{\mathrm{r},1} - L^{\mathrm{p}}_{\mathrm{r},1}$	49.50 dB
System noise temperature: $T_{\mathrm{s},1}$	381.58 K
Required data rate: ϱ [26]	100.00 Mbps
Required signal-to-noise ratio per bit: $(E_{\mathrm{b}}/N_0)^{\mathrm{r}}$ [26]	-2.85 dB
Available signal-to-noise ratio per bit: $(E_{\mathrm{b}}/N_0)^{\mathrm{a}}_1 = \mathrm{EIRP}_1 - L^{\mathrm{a}}_1 + G^{\mathrm{e}}_{\mathrm{r},1} + 228.60 - 10\log_{10} T_{\mathrm{s},1} - 10\log_{10}\varrho$	2.62 dB
Implementation losses: L^{i} [26]	1.35 dB
System Margin: $\mathrm{SM}_1 = (E_{\mathrm{b}}/N_0)^{\mathrm{a}}_1 - (E_{\mathrm{b}}/N_0)^{\mathrm{r}} - L^{\mathrm{i}}$	4.12 dB

Table 2
Link budget for task 2 (intersatellite communication).

Spacecraft and transmitting (designed) antenna	
Input power: P	0.00 dBW
Line losses: L^{l}	0.10 dB
Maximum antenna gain: $G_{\mathrm{t},2}$	13.28 dB
Antenna HPBW: $\Omega_{\mathrm{t},2}$	20.00°
Antenna polarization losses: $L^{\mathrm{x}}_{\mathrm{t},2}$ [21]	0.20 dB
Pointing accuracy: e_{t} [22]	0.50°
Pointing losses: $L^{\mathrm{p}}_{\mathrm{t},2} = 12(e_{\mathrm{t}}/\Omega_{\mathrm{t},2})^2$ [23]	0.01 dB
Antenna effective gain: $G^{\mathrm{e}}_{\mathrm{t},2} = G_{\mathrm{t},2} - L^{\mathrm{x}}_{\mathrm{t},2} - L^{\mathrm{p}}_{\mathrm{t},2}$	13.07 dB
$\mathrm{EIRP}_2 = P - L^{\mathrm{l}} + G^{\mathrm{e}}_{\mathrm{t},2}$	12.97 dBW
Intersatellite path	
Average distance: D_2	15.00 km
$\mathrm{FSPL}_2 = 20\log_{10}(4\pi D_2/\lambda)$ [24]	147.33 dB
Total path attenuation: $L^{\mathrm{a}}_2 = \mathrm{FSPL}_2$	147.33 dB
Spacecraft and receiving (designed) antenna	
Maximum antenna gain: $G_{\mathrm{r},2}$	13.28 dB
Antenna HPBW: $\Omega_{\mathrm{r},2}$	20.00°
Antenna polarization losses: $L^{\mathrm{x}}_{\mathrm{r},2}$ [21]	0.20 dB
Pointing accuracy: $e_{\mathrm{r},2}$ [22]	0.50°
Pointing losses: $L^{\mathrm{p}}_{\mathrm{r},2} = 12(e_{\mathrm{r},2}/\Omega_{\mathrm{r},2})^2$ [23]	0.01 dB
Antenna effective gain: $G^{\mathrm{e}}_{\mathrm{r},2} = G_{\mathrm{r},2} - L^{\mathrm{x}}_{\mathrm{r},2} - L^{\mathrm{p}}_{\mathrm{r},2}$	13.07 dB
System noise temperature: $T_{\mathrm{s},2}$	109.98 K
Required data rate: ϱ [26]	100.00 Mbps
Required signal-to-noise ratio per bit: $(E_{\mathrm{b}}/N_0)^{\mathrm{r}}$ [26]	-2.85 dB
Available signal-to-noise ratio per bit: $(E_{\mathrm{b}}/N_0)^{\mathrm{a}}_2 = \mathrm{EIRP}_2 - L^{\mathrm{a}}_2 + G^{\mathrm{e}}_{\mathrm{r},2} + 228.60 - 10\log_{10} T_{\mathrm{s},2} - 10\log_{10}\varrho$	6.90 dB
Implementation losses: L^{i} [26]	1.35 dB
System Margin: $\mathrm{SM}_2 = (E_{\mathrm{b}}/N_0)^{\mathrm{a}}_2 - (E_{\mathrm{b}}/N_0)^{\mathrm{r}} - L^{\mathrm{i}}$	8.40 dB

5. Conclusions

A reconfigurable antenna array for Ka-band CubeSats has been presented. The proposed structure provides interesting benefits in terms of bandwidth, polarization purity, and versatility, which suggest promising possibilities for the array technology in forthcoming Ka-band nanosatellites. The obtained encouraging results may be strengthened observing that the elements put beside the designed antenna system and adopted to develop the link budgets for a dual-task mission are not high-end components. Hence, low-cost arrays may certainly cooperate with the currently available off-the-shelf devices, thus maintaining the cost-effective requirement of the CubeSat communication system.

Further in-depth analyses might be inferred after the investigation of the impact of the manufacturing tolerances on a physical device, whose realization may be however trustfully carried out on the basis on the here discussed feasibility study and of the fabricated subarray prototype. In conclusion, the flexibility of arrays in providing advanced functionalities combined with the recent innovations in the other related CubeSat technologies, such as ADCSs and miniaturized Ka-band transponders, may represent a really inviting opportunity to accomplish multi-task missions at reasonable costs and reduced deployment risks.

Acknowledgements

This work is partly supported by the Italian Ministry of University and Research (MIUR) within the project FRA 2015 (University of Trieste, Italy), entitled “Peer-to-peer Millimeter-Wave Communications in 5G Networks: Theoretical Modeling and Algorithms for Massive MIMO Systems.” The authors would also like to thank Prof. Federico Alimenti for the helpful support in the experimental development of the subarray feed.

References

[1] California Polytech. State Univ., CubeSat design specif.: Rev. 13, 2015.
[2] R. Hevner, W. Holemans, J. Puig-Suari, R. Twiggs, An advanced standard for CubeSats, in: Proceedings of the AIAA/USU Conf. Small Satellites, 2011.
[3] M.A. Viscio, N. Viola, S. Corpino, F. Stesina, S. Fineschi, F. Fumenti, C. Circi, Interplanetary CubeSats system for space weather evaluations and technology demonstration, Acta Astronaut. 104 (2014) 516–525.
[4] A. Canabal, R.P. Jedlicka, A.G. Pino, Multifunctional phased array antenna design for satellite tracking, Acta Astronaut. 57 (2005) 887–900.
[5] A. Babuscia, B. Corbin, M. Knapp, R. Jensen-Clem, M. van de Loo, S. Seager, Inflatable antenna for cubesats: motivation for development and antenna design, Acta Astronaut. 91 (2013) 322–332.
[6] F. Tubbal, R. Raad, K. Chin, A survey and study of planar antennas for pico-satellites, IEEE Access 3 (2015) 2590–2612.
[7] J.F. Sauder, N. Chahat, R. Hodges, E. Peral, Y. Rahmat-Samii, M. Thomson, Designing, building, and testing a mesh Ka-band parabolic deployable antenna (KaPDA) for CubeSat, in: Proceedings of the AIAA Aerospace Sciences Meet., 2015.
[8] J.A. King, K. Leveque, M. Bertino, J. Kim, H. Aghahassan, Ka-band for CubeSats, in: Proceedings of the AIAA/USU Conf. Small Satellites, 2015.
[9] R.E. Hodges, D.J. Hoppe, M.J. Radway, N.E. Chahat, Novel deployable reflectarray antennas for CubeSat communications, in: Proceedings of the IEEE MTT-S Int. Microw. Symp., 2015.
[10] R.L. Haupt, Y. Rahmat-Samii, Antenna array developments: a perspective on the past, present and future, IEEE Antennas Propag. Mag. 57 (1) (2015) 86–96.
[11] A. Babuscia, K.-M. Cheung, D. Divsalar, C. Lee, Development of cooperative communication techniques for a network of small satellites and CubeSats in deep space: the SOLARA/SARA test case, Acta Astronaut. 115 (2015) 349–355.
[12] C. Underwood, S. Pellegrino, V.J. Lappas, C.P. Bridges, J. Baker, Using CubeSat/micro-satellite technology to demonstrate the Autonomous Assembly of a Reconfigurable Space Telescope (AAReST), Acta Astronaut. 114 (2015) 112–122.
[13] PicoSaTs CubeSat Enterprise. (last access: 21st Feb. 2017). [link] URL ⟨http://picosats.eu/⟩.
[14] R. Martinez Rodriguez-Osorio, E.Fueyo Ramírez, A hands-on education project: antenna design for inter-CubeSat communications, IEEE Antennas Propag. Mag. 54 (5) (2012) 211–224.
[15] R. Garg, P. Bhartia, I. Bahl, A. Ittipiboon, Microstrip antenna design handbook, Artech House Antennas and Propagation Library, 2001.
[16] P.S. Hall, J. Huang, E. Rammos, A. Roederer, Gain of circularly polarised arrays composed of linearly polarised elements, Electron. Lett. 25 (2) (1989) 124–125.
[17] J. Huang, A. Ka-band, circularly polarized high-gain microstrip array antenna, IEEE Trans. Antennas Propag. 43 (1) (1995) 113–116.
[18] A. Chen, Y. Zhang, Z. Chen, C. Yang, Development of a Ka-band wideband circularly polarized 64-Element microstrip antenna array with double application of the sequential rotation feeding technique, IEEE Antennas Wirel. Propag. Lett. 10 (2011) 1225–1536.
[19] M. Comisso, R. Vescovo, Fast iterative method of power synthesis for antenna arrays, IEEE Trans. Antennas Propag. 57 (7) (2009) 1952–1962.
[20] G. Buttazzoni, R. Vescovo, An efficient and versatile technique for the synthesis of 3D copolar and crosspolar patterns of phase-only reconfigurable conformal arrays with DRR and near-field control, IEEE Trans. Antennas Propag. 62 (4) (2014) 1640–1651.
[22] Clyde Space. (last access: 21st Feb. 2017). URL ⟨https://www.clyde.space/⟩.
[25] Comtech Telecommunications Corp., (last access: 21st Feb. 2017). URL ⟨http://www.telecomsys.com/⟩.
[26] European Space Agency, ARTES 5.1 Statement of work: Miniaturised Ka-band FSS transponder for small satellites 5E.001, 2015.
[27] ETSI DVB-S2X Draft Std, Digital Video Broadcasting (DVB); Second generation framing structure, channel coding and modulation systems for broadcasting, interactive services, news gathering and other broadband satellite applications; Part 2: DVB-S2 Extensions, 2014.
[28] M. Mc Nicholas, J. De Luna, R. Manno, Y.-H. Shu, Low cost Ka-band transmitter for CubeSat systems, in: Proceedings of the IEEE Topic. Work. Internet of Space, 2017.
[29] 18 GHz Microwave PLL Synthesizer, Analog Devices. (last access: 21st Feb. 2017). URL ⟨http://www.mouser.com/pdfdocs/ADF41020.pdf⟩.
[30] SWIFT-KTX: High Throughput Software-Defined K-band Communications, Tethers Unlimited, Inc., (last access: 21st Feb. 2017). URL ⟨http://www.tethers.com/SpecSheets/Brochure_SWIFT_KTX.pdf⟩.

Further reading

[1] A.C. Ludwig, A simple graph for determining polarization loss, Microw. J. 19 (9) (1976) 63.
[2] W.J. Larson, J.R. Wertz, Space Mission Analysis and Design, Microcosm Press Springer, 1999.
[3] Centre Nat. Etudes Spatiales, ITU-R Propag. models software library, 2010.

Giulia Buttazzoni received the Laurea degree (summa cum laude) in Telecommunication Engineering and the Ph.D. degree in Information Engineering from the University of Trieste (Italy), in 2008 and 2013, respectively. She is currently a researcher at the Department of Engineering and Architecture of the University of Trieste. Her research interests involve antenna array synthesis and numerical methods for electromagnetic fields.

Massimiliano Comisso received the Laurea degree in Electronics Engineering and the Ph.D. degree in Information Engineering from the University of Trieste (Italy). He worked for Alcatel on optical systems, with Enteos on patch antenna design, and with Danieli Automation on electromagnetic sensor modeling. Currently, Massimiliano Comisso is an Assistant Professor at the Department of Engineering and Architecture of the University of Trieste. His research interests involve smart antenna systems, array synthesis, small antennas, and distributed wireless networks.

Alessandro Cuttin received the Laurea degree in Telecommunication Engineering at the University of Trieste (Italy), where he is currently pursuing the Ph.D. in Information Engineering. He has been with Esteco in 2014, fellow of the National Institute for Astrophysics (INAF) in 2008, and deputy project manager of the AtmoCube team. His research interests involve antenna arrays for LEO satellites and multi-objective optimization.

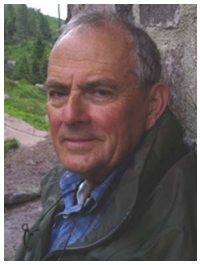

Mario Fragiacomo has been project leader and R & D director at IRET and with Selenia (then Selex Sistemi). He has also been consultant at Mywave Electronics, R & D director at Enteos, co-founder and R & D director at Telital (then, Telit Communications), where he was involved in the design and manufacturing of RTMS, TACS, GSM, GPRS, Globalstar, and UMTS mobile terminals. Mario Fragiacomo received the Honoris Causa degree in Electronics Engineering from the University of Trieste (Italy), in 1999. Currently, as co-founder, he is member of the board at PicoSaTs.

Roberto Vescovo received the Laurea degree, summa cum laude, in Electronic Engineering from the University of Trieste (Italy), in 1982, and the Ph.D degree in Electronics and Information Engineering from the University of Padova (Italy), in 1987. He served as an Assistant Professor at the Department of Engineering and Architecture of the University of Trieste, where he is currently an Associate Professor of Electromagnetic Fields. His main research interests are the synthesis of antenna arrays, the electromagnetic theory, the electromagnetic scattering with related theoretical and computational aspects, and the study of interaction between electromagnetic fields and relativistic electrons.

Roberto Vincenti Gatti received the Laurea degree summa cum laude from the University of Perugia (Italy), in 2000, and the Ph.D. degree from the same University in 2007. Since 2007 he is an Assistant Professor at the University of Perugia. Along the years he headed several industrial and research projects attaining a profound know-how and experience in the area of phased array antennas and RF passive microwave systems. His current research activities include the analysis, modeling and design of slotted waveguide arrays, phased arrays and reflectarrays, phase-only and phase/amplitude synthesis and optimization techniques for planar and conformal arrays, design of passive microwave and millimeter-wave components.